Organic & Biomolecular Chemistry

Cite this: *Org. Biomol. Chem.*, 2011, **9**, 701

www.rsc.org/obc

PAPER

Structural basis for the potential antitumour activity of DNA-interacting benzo[*kl*]xanthene lignans†

Simone Di Micco,[a] Frédéric Mazué,[b] Carmelo Daquino,[c] Carmela Spatafora,[c] Dominique Delmas,[b] Norbert Latruffe,[b] Corrado Tringali,[c] Raffaele Riccio[a] and Giuseppe Bifulco*[a]

Received 23rd July 2010, Accepted 29th September 2010
DOI: 10.1039/c0ob00480d

The biological properties and possible pharmacological applications of benzo[*kl*]xanthene lignans, rare among natural products and synthetic compounds, are almost unexplored. In the present contribution, the possible interaction of six synthetic benzo[*kl*]xanthene lignans and the natural metabolite rufescidride with DNA has been investigated through a combined STD-NMR and molecular docking approach, paralleled by *in vitro* biological assays on their antiproliferative activity towards two different cancer cell lines: SW 480 and HepG2. Our data suggest that the benzo[*kl*]xanthene lignans are suitable lead compounds for the design of DNA selective ligands with potential antitumour properties.

1. Introduction

In current literature, the term 'lignans' is commonly employed to indicate a large family of widespread natural products, biosynthetically originated from the shikimate pathway by oxidative coupling of two phenylpropanoid (C_6C_3) units, displaying an impressive structural diversity and a comparable variety of biological activities. Strictly speaking, lignans are dimers generated by β-β' (8-8′) oxidative coupling of two cinnamic acid residues; this term was originally employed by Haworth[1] and refers to the wood from which many of the first specimens were obtained. However, many other related compounds (neolignans, oxyneolignans, hybrid lignans and others) with a carbon linkage between two C_6C_3 units different from 8-8′, or even with different constitutive monomers, are normally included in this family, as described in recent reviews.[2,3]

Lignans have been found in various plant parts, such as roots, stems, bark, leaves, seeds, and fruits. Some kind of lignans (enterolactones and enterodiols) have been found in mammals, but these are actually metabolic products deriving from a dietary consumption of plant lignans. The biological role of lignans in plant tissues is reasonably related to plant defense, as suggested by their antimicrobial, antifungal, antifeedant, and insecticidal properties. However, in many cases the bioactivities displayed by these plant secondary metabolites are of pharmacological significance, and include antitumor, antioxidant, anti-inflammatory, antileishmanial, antiangiogenic, cardiovascular and antiviral activity.[4–11] A frequently cited example of bioactive lignan, whose chemical modification has led to new useful drugs, is podophyllotoxin (**1**). This natural product is known to be a constituent of *Podophyllum peltatum* since 1880, and recognized as an antitumor compound since around 1950;[12] from the variety of synthetic podophyllotoxin analogues, the anticancer drugs etoposide (**2**), etopophos (**3**) and teniposide (**4**) have emerged.[13]

The biological activities and the structural variety of lignans and related compounds make them an attractive target for chemical synthesis or modification. Although a variety of synthetic methodologies have been employed to this purpose, dimerization reactions carried out through a radical phenolic oxidative coupling of natural precursors, may afford 'unnatural' products by a mechanism mimicking the 'natural' biosynthetic process.[14] These biomimetic syntheses can allow us, in principle, to obtain compounds unprecedented in literature although maintaining a basic 'natural' skeleton and possibly offering a bioactivity profile similar to, or better than, that of a natural analogue. A limit of this synthetic approach is that the lack of stereocontrol both in metal or enzyme mediated phenolic radical coupling[15] frequently results in complex mixtures and racemic compounds. Nevertheless, a number of interesting products have been obtained in such a way, and in some cases the bioactive racemate has been resolved to obtain the most active enantiomer. Thus, some of us have recently carried out the biomimetic synthesis of natural and 'unnatural' lignans by oxidative coupling of caffeic esters, namely CAPE (caffeic acid

[a]*Dipartimento di Scienze Farmaceutiche, Università degli Studi di Salerno, Via Ponte Don Melillo, 84084, Fisciano (SA), Italy. E-mail: bifulco@unisa.it; Fax: +39 089 969602; Tel: +39 089 969741*

[b]*INSERM U 866, University of Burgundy, Laboratory of Biochemistry of Metabolism and Nutrition, 6, Bd Gabriel, F-21000, Dijon, France*

[c]*Dipartimento di Scienze Chimiche, Università degli Studi di Catania, Viale A. Doria 6, I-95125, Catania, Italy*

† Electronic supplementary information (ESI) available: DF-STD NMR spectra for compounds **9**, **10** and **16**, acquired at 300 K (pH 7.1); calculated inhibition constant of the complex formed by **7**–**12** and **16** with models A and B; 3D interactions of **7**–**9**, **11**, **12** and **16** with models A and B; graphical representation of SW480 and HepG2 cells percentages related to the untreated control cells after a 48 h treatment with **8**, **9**, **11** and **12**; phase contrast microscopy observation of SW480 colon cancer cells treated for 48 h with **10**, **11** and **12**; three-dimensional coordinates of models A and B; ^{1}H, ^{13}C and ESI-MS spectra of new compounds **8**, **9** and **11**. See DOI: 10.1039/c0ob00480d

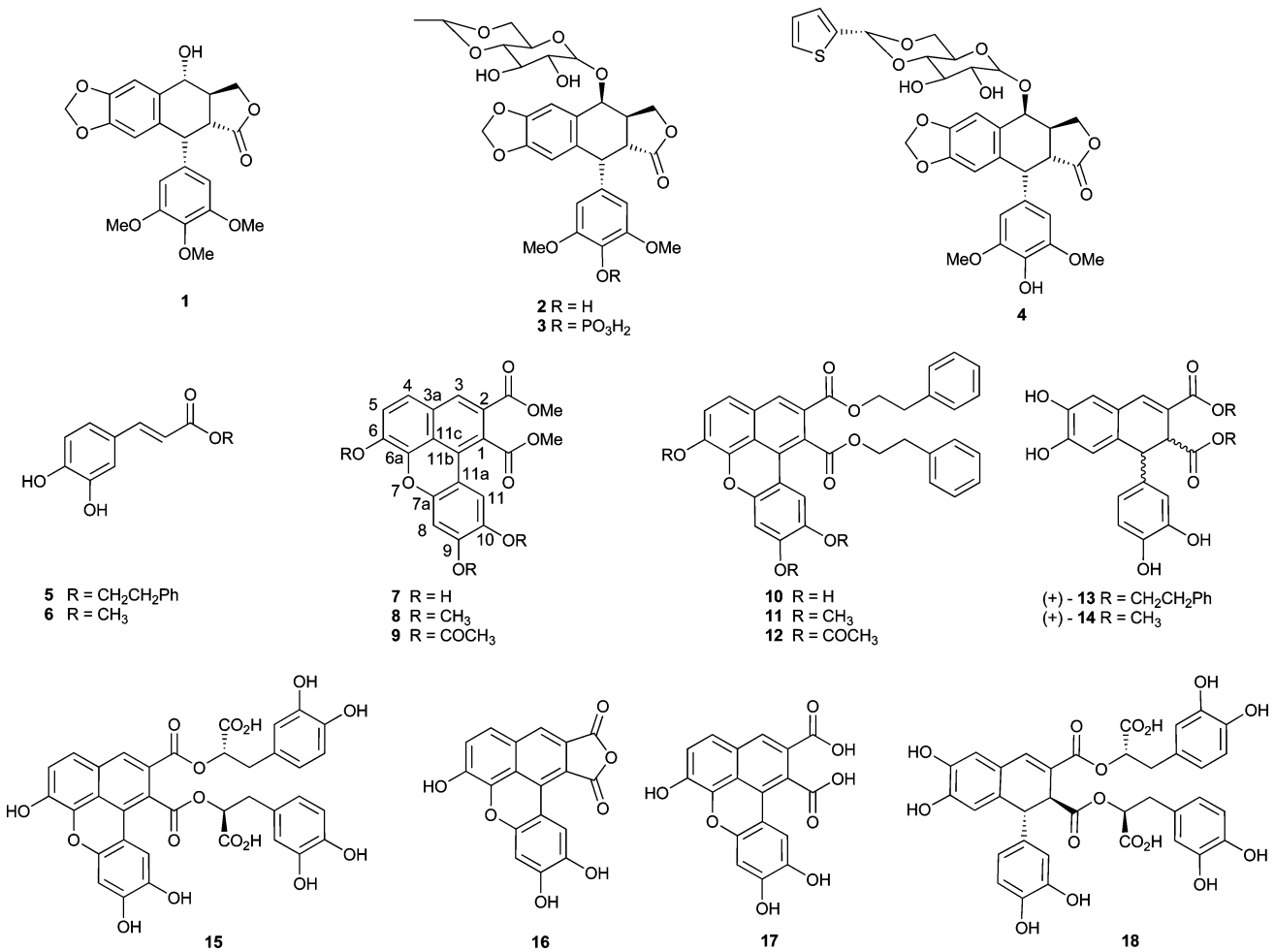

Scheme 1 Molecular structures of podophyllotoxin (**1**), etoposide (**2**), etopophos (**3**), teniposide (**4**), caffeic acid phenethyl ester (CAPE, **5**), caffeic acid methyl ester (**6**) and natural and 'unnatural' lignans **7**–**18**.

phenethyl ester, **5**, Scheme 1) and methyl caffeate (**6**, Scheme 1).[16] CAPE, a well-known component of propolis reported as an anti-inflammatory, antioxidant and antitumor agent,[17a–d] was initially selected because it had never been employed in phenolic oxidative coupling reactions, and unreported dimerization products were expected. The reaction, when carried out on **5** or **6** with $Mn(AcO)_3$ as oxidative reagent, afforded with good yields (72% for CAPE dimerization) the unusual, achiral benzo[*kl*]xanthene lignans **7** and **10** as the main products, accompanied by minor amounts of the aryldihydronaphtalene racemic lignans (±)-**13** and (±)-**14**, respectively.

Benzo[*kl*]xanthene lignans are very rare both among natural products and synthetic analogues. Recently reported representatives are yunnaneic acid H (**15**), rufescidride (**16**) and mongolicumin A (**17**) isolated respectively from *Salvia yunnanensis*,[18] *Cordia rufescens*,[19] and *Taraxacum mongolicum*.[20] Interestingly, the aryldihydronaphtalene lignan rabdosiin (**18**), was also isolated from *S. yunnanensis*,[18] and both are dimers of rosmarinic acid and strictly related respectively to compounds **7** and (±)-**13**, thus indicating the biomimetic nature of our synthetic approach. We also carried out a mechanistic study of this oxidative coupling reaction, and we applied this methodology to synthesize the natural benzoxanthene lignans **16** and **17**.

The lignans **7** and **10** are strongly fluorescent and are also attractive in view of their partly planar structure with extensive conjugation. It is also worth noting that, due to their rarity in nature and the low yield of previous synthetic reactions to obtain analogues,[21a–b] benzoxanthene lignans are almost unexplored with regard to their biological properties and possible pharmacological applications. Even for the previously known rufescidride (**16**, Scheme 1), the only available reference about its biological properties is, to the best of our knowledge, a patent referring to its antimicrobial activity.[22] Thus, as the first step in a study of the putative biomedical properties of these lignans, we have carried out an evaluation of their possible interaction with DNA through an NMR based approach and molecular docking, paralleled by *in vitro* biological assays on their antiproliferative activity towards two different cancer cell lines, namely SW 480 (human colon carcinoma) and HepG2 (human hepatoblastoma). The binding mode of **7**–**12** and **16** to DNA has been analysed by means of the differential frequency-saturation transfer difference (DF-STD)[23] protocol, based on STD-NMR experiments.[24] Along with the NMR binding assays, molecular docking calculations have been performed to get the three-dimensional complex of putative ligands and DNA, to get insights on the structural elements responsible for the affinity to the biological target.

2. Results and discussion

The aim of this work was firstly to evaluate both the possible interaction with DNA and the antiproliferative activity of the benzoxanthene lignans **7–12** and **16**. However, we planned to try to establish at least a minimum of structure–activity relationships for these lignans, and primarily to acquire data about the possible role of the phenolic groups. To this purpose, we prepared by simple chemical conversions carried out on **7** and **10**, respectively the permethyl derivatives **8** and **11** and the peracetyl derivatives **9** and **12**. This small panel of seven compounds was submitted to the DNA interaction and antiproliferative activity studies, as detailed below.

2.1. DF-STD analysis

The experimental STD-NMR outcomes revealed for **7**, **9**, **10** and **16** a binding event with the DNA. Indeed, the appearance of ligand signals in the difference spectra suggested an interaction with the biopolymer. On the other hand, compounds **8** and **11** did not show any STD effects in the recorded spectra, suggesting a very weak interaction with the DNA or a completely absent recognition by the nucleic acid. NMR data were not collected for compound **12**, due to problems of solubility at experimental conditions, and possibly leading to erroneous interpretations of the outcomes.

In order to detect the possible binding mode and to understand the binding contacts of **7–11** and **16** on the DNA surface, the DF-STD[23] protocol was applied, using a poly(dG-dC)·poly(dG-dC) copolymer as biological target. This method consists in the acquisition of a set of STD-NMR[24] experiments at two different saturation frequencies, providing useful information on the binding mode of DNA interacting molecules, discriminating among base-pair intercalators, minor groove binders, and external backbone binders. The comparison of the STD effects at two different saturation frequencies relative to diagnostic protons was performed through the calculation of the binding mode index (BMI),[23] using the following equation:[23]

$$BMI = \frac{\sum_i \left(\frac{SN_{aromatic}/SN_{rif}}{SN_{aliphatic}/SN_{rif}} \right)}{n_i} \quad (1)$$

The BMI is a numerical parameter that, accounting the relative intensities of STD effects at different saturation frequencies, gives insights on binding contacts of the ligands on the DNA surface.[23] In our original contribution, based on the analysis of ligands with a well known binding mode to DNA, we defined three BMI ranges: $0 < BMI < 0.50$ for external (nonspecific) electrostatic backbone binding; $0.90 < BMI < 1.10$ for minor groove binding; and $1.20\ (0.90) < BMI < 1.50$ for base-pair intercalation.[23]

For **7**, **9**, **10** two distinct binding mode indexes (Table 1) were calculated: the BMI relative to the polycyclic aromatic portion, and the BMI′ belonging the chemical appendages in the positions 1, 2, 6, 9 and 10 of the small molecules. Structural consideration on the small molecules prompted us to calculate two BMI, as described for the doxorubicin[23] in our original contribution on DF-STD and recently reported by Gomez-Monterrey *et al.* for the analysis of DNA-interacting spiro derivatives:[25] the presence of a planar conjugated moiety typical of DNA intercalators with flexible substituents.

Table 1 Binding mode index values for **7**, **9**, **10** and **16** calculated by the eqn (1)[23]

Compound	BMI	BMI′
7	1.2	0.7
9	1.0	0.9[a]
		0.6[b]
		0.2[c]
10	1.4	0.8
16	0.9	—

[a] BMI′ calculated for the sole acetoxy in the position 6. [b] BMI calculated for the acetoxy in the positions 9 and 10. [c] BMI calculated for the methoxy groups in the positions 1 and 2.

The DF-STD analysis of **7** (Fig. 1) revealed that the polycyclic aromatic portion intercalates between base pairs of the nucleic acid (BMI, Table 1), whereas the methoxy groups are positioned in the minor groove of the biological target (BMI′, Table 1).

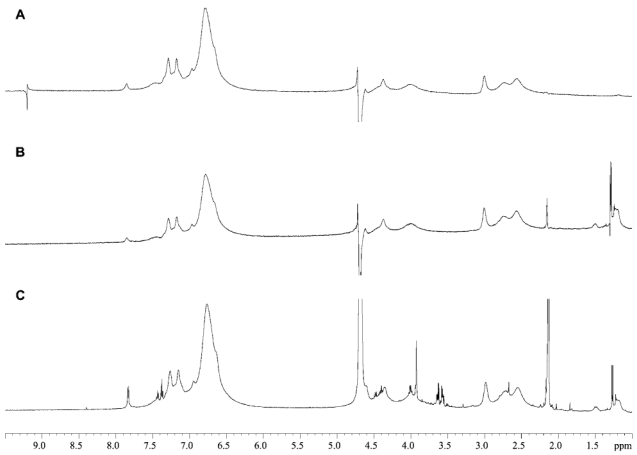

Fig. 1 DF-STD spectra of the **7**-DNA complex. A, B) STD spectra recorded upon saturation in the aromatic (9.0 ppm) and deoxyribose/backbone (2.0 ppm) spectral regions, respectively. C) Reference STD spectrum with an off-resonance irradiation (–16 ppm).

In particular, the BMI value (Table 1) showed a more efficient saturation diffusion irradiating on the purine/pyrimidine resonances, compared to the observed STD effects saturating the deoxyribose/backbone protons (BMI = 1.2), suggesting for the planar structural portion of **7** an intercalation between the bases of DNA (Fig. 1). The BMI value of 1.2 is in fact consistent with data reported for well known DNA intercalators such as thiazole orange (BMI = 1.4)[23] and with the polycyclic aromatic moiety of doxorubicin (BMI = 1.33).[23] Moreover, this value agrees with the BMI of 1.3 obtained for ethidium bromide stacking between base pairs of the parallel quadruplex structure $[d(TGGGGT)]_4$.[26]

The BMI′ of 0.7 revealed a minor groove binding mode of the aliphatic portion of **7**; such a value is in accordance with similar values obtained for well known minor groove binders, such as distamycin A (BMI = 1.1) and netropsin (BMI = 0.9).[23] The BMI′ is also similar to the experimental data describing the interaction of distamycin A with the minor groove of a DNA quadruplex (BMI = 0.8).[26]

The structural difference between **7** and **10** relates to the presence of two phenylethyl groups in positions 1 and 2 (Scheme 1). However, similar interactions with the biological target were

observed. Indeed, the obtained binding mode indexes were comparable to the values found for **7**. The BMI (1.4, similar to the value of **7**) confirmed the base pairs intercalation, because the intensities of the STD effects are higher irradiating aromatic proton resonances of the nucleic acid (Figure S1†). As observed for **7**, the BMI′ (0.8, Table 1) is the result of a similar saturation diffusion efficiency by differential irradiation of the purine/pyrimidine bases and the deoxyribose/backbone spectral regions (Figure S1).

Compound **9** is the three-acetylated derivative of **7** at the positions 6, 9 and 10. While the expected binding mode of **9** is similar to that of compound **7**, as confirmed by a DF-STD approach, the analysis of the experimental data was complicated by the presence of the bulky acetyl groups. Indeed, the steric clashes exerted by acetyl functionalities reduce the maximum overlap with the flanking DNA base pairs giving raise to a BMI value of 1 (Table 1). Concerning the experimental outcomes for the aliphatic moieties of **9**, different BMI′ values were obtained for the contributions of methoxyl and acetyl groups (see Table 1). The experimental data investigation revealed that the acetyl group in position 6 (2.36 ppm, Figure S2†) showed comparable STD effects at two saturation frequencies (BMI′ = 0.9), suggesting an accommodation in the minor groove of the nucleic acid, as found for the ester groups of **7** and **10**. The BMI′ is consistent with the values for well known minor groove binders distamycin A (BMI = 1.1) and netropsin (BMI = 0.9) interacting with the poly(dG-dC)·poly(dG-dC) copolymer[23] and with a BMI of 0.8 for the distamycin A interacting with the minor groove of the $[d(TGGGGT)]_4$ quadruplex.[26] Consequently, the expected location of the other acetyls of compound **9** on the DNA surface is along the major groove, where these groups experienced a similar saturation transfer from aromatic and deoxyribose/backbone proton irradiation (Table 1). The two methoxy groups are accommodated in the major groove of the deoxyribonucleic acid pointing towards the deoxyribose/backbone, and causing a BMI′ value of 0.2. These findings are in agreement with molecular docking calculations (see the next section).

We have also investigated by a DF-STD protocol the possible DNA interactions for compound **16** (Figure S3†). As predicted by the simple inspection of structural planar feature of **16**, its binding mode consists of an intercalation between the base pair aromatic rings of DNA. The experimental data reveal π-stacking interactions with purinic and pyrimidinic bases of the biological target, accompanied by interactions with the external deoxyribose/backbone by the hydroxy groups of **16**. In fact, the obtained BMI of 0.9 is in perfect agreement with the binding mode index calculated for investigated particular intercalator, ethidium bromide, in our original paper.[23] In detail, the ethidium bromide is a base-pairs intercalator, able to interact with external negatively charged phosphate by its amino groups.

2.2. Molecular docking studies

Molecular docking calculations, using AutoDock 3.0.5,[27] were performed to predict a 3D model of the complex between compounds **7**, **9**, **10**, **12**, **16**, and the DNA, to get insights on the structural elements responsible of the binding to the biological target, and for the eventual design of more selective and potent analogues. In the calculations different binding sites were considered, to discriminate the preferred binding mode on the DNA surface (intercalation, minor groove accommodation and deoxyribose/backbone binding) by the potential ligands. Moreover, the study of intercalation between base pairs was performed taking into account two binding cavities (Fig. 2), in order to evaluate if this type of interaction to the DNA, and the consequent hydrogen bond formations, were base-dependent.

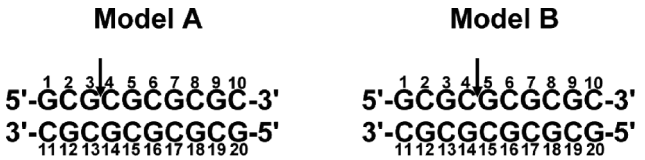

Fig. 2 Schematic representation of DNA models (A and B) used in docking calculations. Sequence and numbering of two 10mers (A and B) DNA duplexes are reported. The arrows indicate the intercalation points.

The analysis of docking calculations, based on visual inspection and scoring function values, revealed that compounds **7–12** and **16** intercalate the DNA with their chromophores and collocate the flexible substituents on different points of the DNA surface, in accordance with the findings obtained by the experimental DF-STD data. As reported in Fig. 3, compound **7** stacks its planar portion between two adjacent base pairs establishing π–π interactions (Fig. 3).

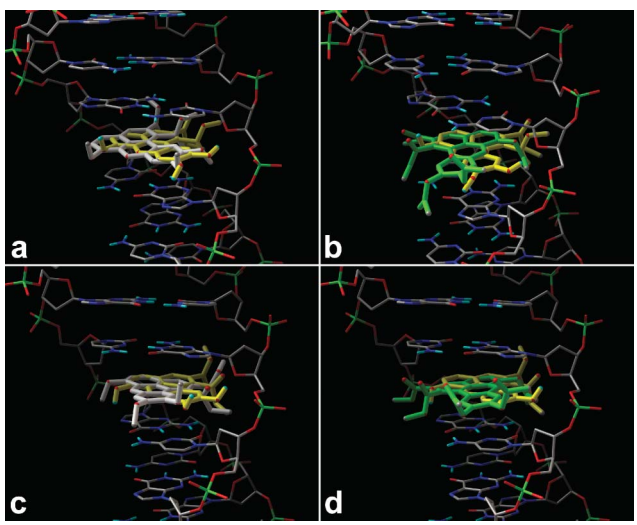

Fig. 3 a) and c) **7** and **8** superimposition in the binding site of models A and B, respectively. b) and d) **7** and **9** superimposition in the binding site of models A and B, respectively. The ligands and DNA are represented by tube, and their atoms coloured by atom type: C, gray; polar H, sky blue; N, blue; O, red. For **7–9**, bonds are depicted respectively in yellow, white and green. The figure highlights the overlap with base pairs and interactions with minor groove.

In our model, the oxygen of ester functionality (position 1, Scheme 1) forms a hydrogen bond with the NH_2 of G14 (Figure S4a†). The hydroxy group in 10 establishes a hydrogen bond with the anomeric oxygen of deoxyribose, whereas the OH in 6 and 9 gives the same type of interaction with N7 of G3 and G14, respectively. The methyl groups point along the minor groove, contributing to the complex stability by means of hydrophobic interactions with the macromolecular counterparts. The comparison of docking calculations performed on models A and B (Figure S4)

showed similar results. The predicted bioactive conformations, indeed, are superimposable, giving the same number of hydrogen bonds with similar distances. In particular, for model B (Figure S4c and d) the docked pose presents a hydrogen bond with carbonylic oxygen of G5 and OH 9, instead of OH 6 as found with model A (Figure S4a and b).

The same considerations apply for compound **10** (Fig. 4).

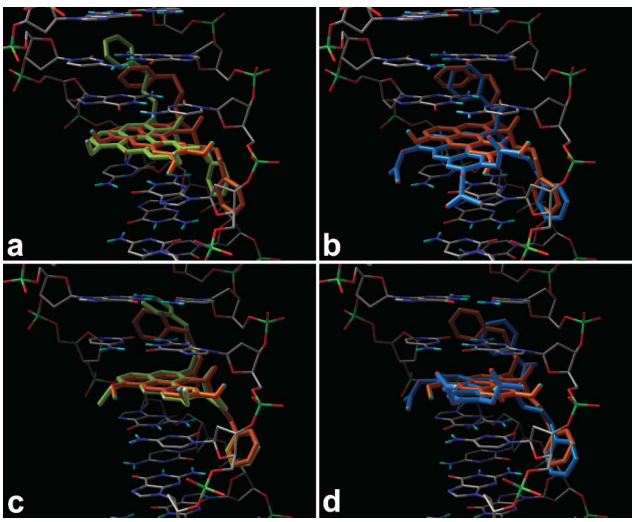

Fig. 4 a) and c) **10** and **11** superimposition in the binding site of models A and B, respectively. b) and d) **10** and **12** superimposition in the binding site of models A and B, respectively. The ligands and DNA are represented by tube, and their atoms coloured by atom type: C, gray; polar H, sky blue; N, blue; O, red. For **10–12**, bonds are depicted respectively in orange, light green and blue. The figure highlights the overlap with base pairs and interactions with minor groove.

Within both models A and B, the common polycyclic aromatic moiety intercalates between base pairs forming π–π interactions with the macromolecular counterparts and the two phenylethyl groups are accommodated along the minor groove establishing van der Waals contacts (Fig. 5). Moreover, for model A, the oxygen of the ester functionality (in position 1, Scheme 1) is involved in a hydrogen bond with the NH_2 (in 2) of G5. As found for **7**, the OH at C-10 (Scheme 1) interacts with the anomeric oxygen of deoxyribose, whereas the hydroxy group at C-9 has a contact with the N7 of G14 (Fig. 5b). For model B, there is a hydrogen bond between OH at C-6 and carbonylic oxygen (at C-6) of G5 (Fig. 5d).

It is noteworthy that, besides the π-stacking, the two common planar portions of compounds **7** and **10** show the same orientation between the two adjacent base-pairs of models A and B. These theoretical results are in agreement with the similar experimental BMI values obtained for **7** and **10** (Table 1).

In contrast to the two methyl substituents of **7**, the phenylethyl groups contribute more efficiently to the complex stability, giving wider van der Waals contacts along the minor groove of the DNA (Table S1†). The difference in the predicted binding affinity for **7** and **10** is due to the presence of these two bulky groups in **10** (Table S1) and these theoretical results are in good qualitative agreement with the biological data (see the next section, Table 2).

The analysis of docking results obtained for **9**, the three-acetylated derivative of **7**, revealed an intercalative binding mode with a different arrangement of the ester groups along the grooves

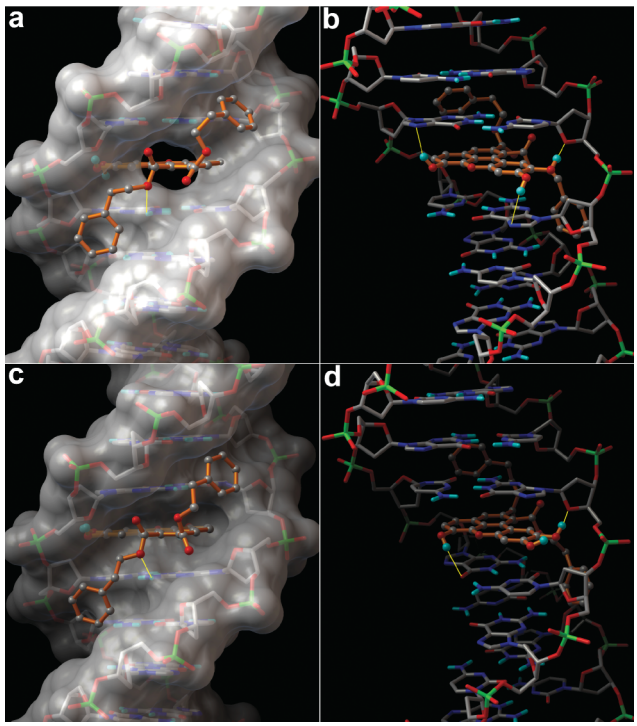

Fig. 5 3D interactions of **10**-model A (a and b) and **10**-model B (c and d) complexes. In a) and c) the DNA is represented by the molecular surface, and sticks and balls (coloured by atom type: O, red; C, grey; polar H, sky blue; N, blue), whereas in b) and d) only by sticks and balls. The ligand is depicted in sticks (orange) and balls (coloured as for DNA). In a) and c), the figure highlights the intercalation between two adjacent base pairs and the hydrogen bonds (yellow line) between ester functionality and NH_2 of guanine. In b) and d), besides the intercalation, the hydrogen bonds (yellow line) formed by OH group are shown.

of the DNA (Fig. 3). The acetyl functionality in position 6 is accommodated in the minor groove giving van der Waals contacts by the methyl and creating a hydrogen bond with the NH_2 of G14 with its carbonyl group. In our theoretical ligand-DNA complex, the remaining ester functionalities lay along the major groove of the nucleic acid (Figure S5†). In detail, the methoxy group in 3 follows the bend of deoxyribose backbone, giving close contact with the external backbone of the DNA, as also outlined by the BMI′ value (Figure S5). The methoxy group in 2 is hydrogen bonded to the NH_2 of C4 and its methyl points toward the solvent. The acetyl group in 10 establishes a hydrogen bond with the NH_2 of C13 and by the oxygen of carbonyl and the methyl group is in contact with the external phosphate backbone and the base pair

Table 2 IC_{50} values (μM) for **7–12** and **16**, obtained on the colon (SW480) and hepatic (HepG2) cancer cells. IC_{50} values calculated after 48 h of continuous exposure relative to untreated controls. Values are the mean ± SD of three experiments

Compound	IC_{50}, (μM, SW480)	IC_{50}, (μM, HepG2)
7	32.89 ± 6.60	34.83 ± 7.15
8	> 100	> 100
9	25.5 ± 9.35	28.61 ± 5.50
10	2.57 ± 0.58	4.76 ± 0.56
11	> 100	≫ 100
12	3.21 ± 0.33	26.66 ± 3.85
16	≫ 100	> 100

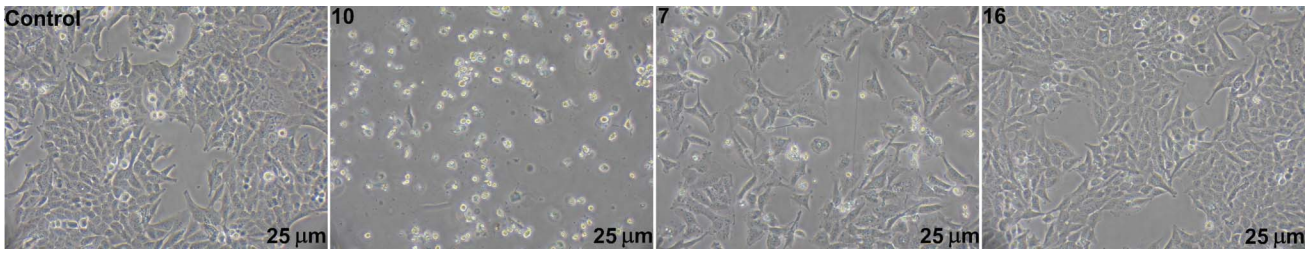

Fig. 6 Phase contrast microscopy observation of SW480 colon cancer cells treated or not for 48 h with 30 μM of **10**, **7** and **16**.

aromatic rings of the DNA (Figure S5). The acetyl in 11 faces the base pairs along the groove floor of the biological target. Similar findings were obtained for model B (Figure S5), where compound **9** shows a similar docked pose compared to the predicted bioactive conformation interacting with model A. In our theoretical model, the acetyl group in 6 is hydrogen bonded through its carbonyl oxygen with the NH_2 of G5, and the methoxy group in 2 establishes a hydrogen contact with the NH_2 of C4.

In the predicted model of the complex formed by the DNA and compound **12**, we observed an overlapping docked pose for **10** and **12** for both models A and B (Fig. 4). In particular, the chromophore is intercalated by two base pairs of the DNA, and the phenylethyl groups establish van der Waals contacts and hydrogen bonds with the minor groove of the biological target, giving a great contribution to the affinity for the macromolecule. In detail, the ester group in 2 appears to be hydrogen bonded with the NH_2 in 7 of G3 and, along with the substituent in 1, it shares a hydrogen bond with the NH_2 of G14 (Figure S6†). The bulkier acetyl groups are accommodated in the wider major groove. The acetyl groups in 6 and 9 are involved in hydrogen bonds with NH_2 of C4 and C13 respectively, with the oxygen of the carbonyl. For model B, two oxygen atoms bounded to the phenylethyl groups, are hydrogen bonded with the NH_2 of G5, whereas the CO in position 9 makes the same interaction with the NH_2 of C15 (Figure S6). Interestingly, the comparison of **9** and **12** with their progenitor **7** and **10**, revealed that the chemical conversion of hydroxy groups in acetoxy functionalities causes the conversion of hydrogen bond donors in acceptors without loss of interaction with macromolecular counterparts (Figure S5 and S6). Indeed, the acetoxy groups, in our predicted models, are hydrogen bonded with nucleotides, as found for the hydroxy groups of **7** and **10** (Figure S5 and S6). Moreover, the bulky acetoxy groups do not favour the maximum overlap with the adjacent aromatic rings of the DNA, as outlined by the BMI value of **9** (Table 1, Fig. 3 and 4). These findings are responsible of a lower predicted binding affinity of **9** and **12**, with respect to **7** and **10** (Table S1). Conversely, the three-methylated derivatives **8** and **11** are not able to establish hydrogen bonds with the nucleotides due to the presence of methyls groups (Figure S7 and S8), causing a lower affinity for the DNA, as also revealed by experimental NMR data and biological assays (Table 2).

Finally, the docking outcomes for **16** were in line with the DF-STD analysis. In fact, we find that **16** establishes extended van der Waals contacts with base-pair aromatic rings, and the hydroxy functionalities in 6 and 9 are hydrogen bonded with anomeric oxygen of deoxyribose ring of nucleotides C13 and C4, respectively (Figure S9†). Similarly, for model B these two hydroxyl groups give hydrogen bonds with nucleotides G14 and G5, and the chromophore intercalates between C4·G14 and G5·C15 base pairs (Figure S9).

2.3. Antiproliferative activities

The antiproliferative activity of lignans **7–12** was evaluated on SW480 (colon) and HepG2 (hepatic) cancer cells. Results, expressed as IC_{50} values, are reported in Table 2. The most active compound was the benzoxanthene lignan **10**, potently active both on colon ($IC_{50} = 2.57$ μM) and hepatic cancer cells ($IC_{50} = 4.76$ μM). Also the three-acetylated derivative **12** strongly inhibits the cellular proliferation after a 48 h treatment, selectively on colon cells ($IC_{50} = 3.21$ μM), and to a lesser extent, on hepatic cells ($IC_{50} = 26.66$ μM). It is worth noting that compounds **10** and **12**, bearing the phenylethyl pendants at positions 1 and 2, are significantly more active than compounds **7** and **9**, which have methyl ester groups in the same positions. The chemical conversion of the hydroxy into methoxy groups in compounds **8** and **11** dramatically decreases the cytostatic effect of the original molecules (**7** and **10**), indicating a fundamental role of hydroxy or acetoxy groups in the antiproliferative activity. Also rufescidride (**16**), lacking any pendant group, exhibited poor activity. This is evident in Fig. 6 were the optical microscopy images of SW480 colon cancer cells are reported after a 48 h treatment with 30 μM of **7**, **10** and **16** in comparison with the control culture. Also graphs in Fig. 7 clearly indicate the different activity of these three structurally related benzoxanthenes, as shown by the viability cell curves of both SW480 and HepG2 cells treated with increasing concentrations of the three compounds.

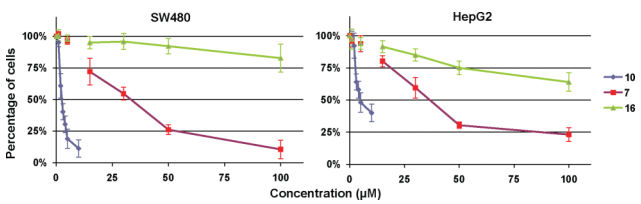

Fig. 7 Graphical representation of SW480 (left) and HepG2 (right) cell percentages related to the untreated control cells after a 48 h treatment with **7**, **10** and **16**. Counting is realized with a haemocytometer after dead cells exclusion by Trypan Blue staining.

These finding corroborate the structural considerations reported above, obtained from molecular docking studies and NMR experiments, highlighting the crucial role of phenylethyl groups on the affinity for the DNA as well as the importance of hydroxyl groups in the DNA binding. Moreover, the activity of

three-acetylated derivatives, comparable to that of the parent molecules, could be explained by a better cell membrane penetration and the hydrolytic action of cellular esterases, releasing the hydroxylated compounds **7** and **10**. The importance of the pendant groups in **7** and **10** is confirmed by the scarce antiproliferative activity of rufescidride (**16**). The detected binding to DNA by NMR experiments could be in accordance with the antimicrobial activity of **16** recently reported in a patent.[22]

3. Experimental

3.1. General

All chemicals were of reagent grade and used as purchased from Sigma-Aldrich. LiChroprep Si-60 and LiChroprep DIOL 25-40 (Merck) were used as stationary phases for column chromatography. TLC was carried out using pre-coated silica gel F_{254} plates (Merck). Cerium sulfate and phosphomolybdic acid were used as spray reagents. ESI-MS spectra were carried out on mass spectrometer Agilent MS G1956A. NMR spectra were run on a Varian Unity Inova spectrometer operating at 499.86 (^{1}H) and 125.70 MHz (^{13}C) and equipped with gradient-enhanced, reverse-detection probe. Chemical shifts (δ) were indirectly referred to TMS using solvent signals. STD-NMR experiments were performed on a Bruker Avance DRX 600-MHz spectrometer, equipped with cryoprobe, at 300 K (see below for details).

3.1.1. Synthesis of compounds 7, 10, 12 and 16

Dimethyl 6,9,10-trihydroxybenzo[*kl*]xanthene-1,2-dicarboxylate (**7**), bis(2-phenylethyl)-6,9,10-trihydroxybenzo[*kl*]xanthene-1,2-dicarboxylate (**10**), bis(2-phenylethyl) 6,9,10-tris(acetyloxy)-benzo[*kl*]xanthene-1,2-dicarboxylate (**12**) and rufescidride (**16**) were synthesized as previously described.[16]

3.1.2. Bis(2-phenylethyl)-6,9,10-trimethoxybenzo[*kl*]xanthene-1,2-dicarboxylate (11)

Compound **10** (32 mg, 0.056 mmol) was placed into a boiling flask and dispersed in 10 mL of acetone and 25 mg of anhydrous potassium carbonate. To this suspension 20 µl of dimethyl sulfate was added. The resulting mixture was heated for 18 h under a reflux condenser. Acetone was then removed by a rotary evaporator and the residue was purified by LC (silica gel, $CHCl_3$ in *n*-hexane from 70% to 75%) so as to obtain 32.5 mg (94.6% yield) of **11**: yellow amorphous powder; R_f (TLC) = 0.33 (80% $CHCl_3$–*n*-hexane); ^{1}H NMR [500 MHz, $(CD_3)_2CO$, 298 K]: δ 8.12 (s, 1H, 3-H), 7.58 (d, J = 8.5 Hz, 1H, 4-H), 7.54 (d, J = 8.5 Hz, 1H, 5-H), 7.38–7.15 (m, 10H, phenylethyl ring), 7.24 (overlapped with other signals, 1H, 11-H), 6.81 (s, 1H, 8-H), 4.62 (t, J = 9.0 Hz, 2H, 1″-H), 4.47 (t, J = 9.0 Hz, 2H, 1″-H), 4.03 (s, 3H, OCH_3), 3.93 (s, 3H, OCH_3), 3.70 (s, 3H, OCH_3), 3.09 and 3.08 (two t, partly overlapped, J = 7.0 Hz, 4H, 2″-H and 2″-H). ^{13}C NMR [125 MHz, $(CD_3)_2CO$, 298 K]: δ 169.9, 165.6, 152.2, 147.8, 145.8, 144.5, 138.8, 138.2, 138.2, 129.0, 129.2, 128.8, 128.4, 128.3, 127.2, 126.4, 126.3, 125.7, 124.6, 121.3, 123.1, 121.2 120.6, 116.1, 109.9, 108.4, 101.1, 66.3, 65.7, 56.2, 55.7, 55.4, 34.7, 34.3. ESI MS: m/z = 627.1 [M^+ +Na].

3.1.3. Dimethyl 6,9,10-trimethoxybenzo[*kl*]xanthene-1,2-dicarboxylate (8)

Compound **7** (60.6 mg, 0.158 mmol) was treated with dimethyl sulfate using the same procedure described above for **10** to afford a residue which was purified by LC (silica gel, 70% $CHCl_3$ in *n*-hexane) so as to obtain 62.5 mg (93.3% yield) of **8**.

Yellow amorphous powder: R_f (TLC) = 0.42 (100% $CHCl_3$); ^{1}H NMR [500 MHz, $CDCl_3$, 298 K]: δ 8.19 (s, 1H, 3-H), 7.45 (d, J = 8.5 Hz, 1H, 4-H), 7.35 (d, J = 8.5 Hz, 1H, 5-H), 7.29 (s, 1H, 11-H), 6.81 (s, 1H, 8-H), 4.05 (s, 6H, OCH_3), 3.93 (s, 6H, $COOCH_3$), 3.91 (s, 3H, OCH_3). ^{13}C NMR [125 MHz, $CDCl_3$, 298 K]: δ 171.6, 166.4, 151.3, 147.8, 145.5, 143.9, 139.1, 129.4, 127.4, 125.1, 124.9, 123.5, 121.1, 120.4, 115.3, 110.4, 107.5, 101.1, 56.7, 56.2, 56.0, 52.5, 52.1. ESI MS: m/z = 447.0 [M^+ +Na], 462.9 [M^+ +K].

3.1.4. Dimethyl 6,9,10-tris(acetyloxy)benzo[*kl*]xanthene-1,2-dicarboxylate (9)

Compound **7** (26 mg, 0.068 mmol) was dissolved in pyridine (1 mL) and acetic anhydride (1.2 mL). The solution was stirred at room temperature for 4 h and, after standard work-up, the peracetate **9** was obtained with 96% yield. Yellow amorphous powder: R_f (TLC) = 0.35 (100% $CHCl_3$); ^{1}H NMR [500 MHz, $(CD_3)_2CO$, 298 K]: δ 8.4 (s, 1H, 3-H), 7.73 (d, J = 8.5 Hz, 1H, 4-H), 7.52 (d, J = 8.5 Hz, 1H, 5-H), 7.58 (s, 1H, 8-H), 7.23 (s, 1H, 11-H), 3.96 (s, 3H, $COOCH_3$), 3.93 (s, 3H, $COOCH_3$), 2.41 (s, 3H, $COCH_3$), 2.33 (s, 6H, $COCH_3$). ^{13}C NMR [125 MHz, $(CD_3)_2CO$, 298 K]: δ 169.0, 167.9, 167.3, 165.0, 149.7, 144.3, 141.2, 138.8, 134.8, 131.0, 131.1, 130.2, 127.4, 124.9, 123.4, 123.2, 122.9, 121.8, 120.2, 116.3, 112.8, 52.3, 52.1, 19.6, 19.59, 19.57. ESI MS: m/z = 530.9 [M^+ +Na].

3.2. DF-STD NMR

Before running the NMR experiments, the solubility of compounds **7–12** and **16** was evaluated. The mixture of acetone/water containing phosphate buffered saline (10 mM) at pH 7.1 was used to verify the solubility of the molecules. For **7** and **8** the final concentration was 1 mM and for the DNA 50 µM (expressed as molarity of phosphate groups) in 200 µl of solvent: acetone/deuterated water 10/190 for **7** and a ratio of 30/170 for **8**. The concentrations were halved for **9–11** and the DNA with respect to **7** and **8**, using the solvent acetone/deuterated water in the ratios 60/140, 20/180 and 80/120 for **9–11**, respectively. For **16** the final concentration was 1.8 mM and for the DNA 90 µM (expressed as molarity of phosphate groups) in 200 µl of solvent (acetone/deuterated water 20/180).

The DNA used as biological target was a poly(dG-dC)·poly(dG-dC) copolymer (Sigma Aldrich), presenting an average of 750 base pairs. The copolymer was dissolved in the above described buffer aqueous solution and underwent at annealing for 5′ at 80 °C. The copolymer was dried and afterwards dissolved in the deuterated buffer with the percentage of acetone as describe above.

Two STD NMR spectra for each ligand were recorded irradiating on the aromatic and sugar proton resonances of DNA by a Gaussian train pulses reaching a total saturation time of 4 s.

For **7** the saturation frequencies were 9.0 ppm (aromatic spectral region) and 2.0 ppm (sugar spectral region). For **8** and **9** the aromatic DNA protons were irradiated at respectively 9.4 and 9.8 ppm, and the aliphatic resonances at 5.5 ppm. For **10** the

saturation frequencies of 9.2 ppm and 1.3 ppm, and for **11** 9.8 and 1.2 ppm were respectively applied to irradiate aromatic and deoxyribose/backbone spectral regions of the nucleic acid. For **16**, the selective irradiation was applied at 9.4 ppm and 1.2 ppm. The STD effects of the individual protons were calculated for each compound relative to a reference spectrum with off-resonance saturation at $\delta = -16$ ppm.

Typically, 32 scans were recorded for the reference STD spectrum, whereas 64 scans were recorded for each DF-STD spectrum for **7**, **8** and **16**. The numbers of scans were doubled in the set of experiments for **9–11**.

The relative STD effects were calculated for each signal as the difference between the intensity (expressed as an S/N ratio) of one signal in the on-resonance STD spectrum and that of the same signal in the off-resonance NMR spectrum divided by the intensity of the same signal in the off-resonance spectrum. BMI values were obtained by using eqn (1).[23]

3.3. Computational methods

The models of the biological target were built by using the graphical interface Maestro version 6.0, Schrödinger, LLC, New York, NY, 2003. A B-DNA decamer (dG-dC)·(dG-dC) was built, in order to have a complete helix turn, using the available base-pair models of Maestro (see supporting information for the three-dimensional coordinates of the models†). To study the intercalation between base pairs, the binding site was built taking into account the distances from experimental structures of the complex between the nucleic acids and intercalators and the induced local unwinding. In particular, we observed that the experimental distances between the base-pairs ranged from 6.3 Å to 7.6 Å.[28] Considering this range of experimental distances, and applying increments of 0.1 Å to the base-pair distance of our B-DNA duplexes we built different models, finding 6.9 Å as the optimal spacing for the ligand binding. Thus, two intercalations points were built (models A and B), using the found distance of 6.9 Å between base-pairs, and considered in the calculations. In details, the binding site of model A was formed by the G3·C13 and C4·G14 base pairs, whereas for the model B the intercalation point was delimited by C4·G14 and G5·C15 base pairs. Both models were optimized using Macromodel 8.5 software,[29] by Polak-Ribiere Conjugate Gradient method using the Force Field Amber[30] (threshold 0.005 kJ mol^{-1} Å^{-1}). The GB/SA (Generalized Born/surface area)[31] solvent treatment was used, mimicking the presence of H_2O, in the calculations for reducing the artifacts derived from the absence of the solvent. During the optimization of the geometries and energies of models A and B, a penalty of 100 kJ Å^{-2} was applied for the distance violations along the hydrogen bonds between nucleotides aromatic rings of each complementary strand.

All ligands structures were built and their geometries optimized through MacroModel 8.5 software[29] package and using the MMFFs force field.[32] The MonteCarlo Multiple Minimum (MCMM) method (10,000 steps) of the MacroModel package[29] was used in order to allow a full exploration of the conformational space. The so obtained geometries were optimized using the Polak–Ribier Conjugate Gradient algorithm (PRCG, maximum derivative less than 0.001 kcal mol^{-1}). Autodock 3.0.5[27] was used for all docking calculations. The software rapidly takes into account the ligand-macromolecule interactions by precalculating atomic affinity potentials (*grid maps*) for each atom type in the substrate molecule by the grid method.[33] These maps are calculated by AutoGrid, where the protein is embedded in a three-dimensional grid and a probe atom is placed at each grid point. The energy of interaction of this single atom with the protein is assigned to the grid point. Thus, to study the binding mode to DNA, several docking calculations were performed collocating the grid box on different regions of the DNA surface: minor and major groove, along the external backbone and the vertical axes comprising base pairs. For all the docking calculations considering the minor groove as the binding site, a grid box size of $62 \times 62 \times 62$ with spacing of 0.375 Å between the grid points was used and centred on the following x, y and z coordinates: –0.256; 1.561; 15.262. Where the major groove was the binding cavity, a grid box size of $48 \times 56 \times 50$ with a spacing of 0.375 Å between the grid points used and centred on the following x, y and z coordinates: 4.56; 1.561; 15.262. For all the docking calculations with models A and B, a grid box size of $54 \times 54 \times 64$ with spacing of 0.375 Å between the grid points was used and centred on the following x, y and z coordinates: –1.189; 2.505; 21.5. The above described grid boxes also included the external deoxyribose/backbone.

In order to achieve a representative conformational space during the docking calculations on the ligands under investigation, ten calculations consisting of 256 runs were performed, obtaining 2560 ligand conformations (256×10). The Lamarkian genetic algorithm was used for dockings. An initial population of 650 randomly placed individuals, a maximum number of 10×10^6 energy evaluations, and a maximum number of 11×10^6 generations were taken into account. A mutation rate of 0.02, a crossover rate of 0.8 and a local search frequency of 0.26 were used.

All the 3D models were depicted using the Phyton software:[34] molecular surfaces were rendered using Maximal Speed Molecular Surface (MSMS).[35]

3.4. Proliferation assays

All compounds under test (**7–12** and **16**) were dissolved in dimethylsulfoxide (DMSO) solution. Stock solutions were prepared at 100 mM or 10 mM. Solutions were stored at 4 °C avoiding light exposure. The human colon carcinoma cell line SW480 was cultured in RPMI-medium with 10% fetal bovine serum and 1% antibiotics (penicillin and streptomycin from Sigma-Aldrich) and for HepG2 human hepatoblastoma cell line, DMEM +10% fetal bovine serum (FSB) + 1% antibiotics. Cells at 90% confluence were separated with trypsin/EDTA and reseeded at 1/10 (surface/surface) in 12-well plates (final volume of 1 mL RPMI medium for each well). After 24 h, cells were treated in separate experiments with lignans **7–12** and **16** at a final concentration of 0.1% DMSO.

Proliferation inhibition assays were performed in 24-well plates in triplicate, and each experiment was conducted three times. In all, 30,000 cells were seeded per well and after 24 h were treated with media containing either each compound in dimethylsulfoxide (0.1% final concentration) or with 0.1% dimethylsulfoxide as control (0.1% final concentration). After 48 h, adherent cells were collected by trypsinization and washed with 1X PBS.

Counting of living cells was made on Mallassez cells. Dead cells were excluded by coloration with Trypan Blue. Subsequently,

48 h IC_{50} values were determined by performing 1 nM to 100 μM treatments and the IC_{50} values were obtained after parametric regressions on the percentages of viable cells *versus* the control.

3 Conclusions

A significant portion of all anticancer drugs are DNA-interacting molecules, and many clinical anticancer compounds are natural products or their synthetic or semisynthetic derivatives. In the present study the benzoxanthene lignans **7–12** and **16** have been analysed as potential DNA interacting molecules, through DF-STD NMR spectroscopy, and their antiproliferative activity has been tested towards two different cancer cell lines, SW 480 (human colon carcinoma) and HepG2 (human hepatoblastoma). Molecular modeling studies have also been performed to deepen the structure–activity relationships in order to design more potent and selective analogs. In detail, by DF-STD experimental protocol we have monitored the binding events that occur at specific regions of the duplex DNA. The experimental outcomes reveal that the planar chromophoric moiety of the studied compounds is intercalated between two base pairs and the flexible chemical appendages are collocated along the grooves of the nucleic acid and make contacts with the external deoxyribose/backbone. The docking results are in agreement with the experimental NMR data. Indeed, the predicted bioactive conformations of tested compounds present the polyaromatic system establishing π–π interactions with two flanking DNA base pairs and the ester groups give a further contribution to the DNA binding by their van der Waals contacts and hydrogen bonds with macromolecular counterparts. In particular, the bulky phenylethyl groups of **10** and **12**, giving wider van der Waals contacts with the minor groove, improve the binding affinity, as highlighted by the higher calculated inhibition constants and the IC_{50} values of biological data. Our investigation has also highlighted a crucial role of the phenolic groups in the recognition process by the biological target. Indeed, the chemical conversion of the hydroxy into methoxy functionalities prevents the hydrogen bond formation between ligands and macromolecule, lowering the affinity for the DNA, as outlined by our combined strategy of investigation for **8** and **11**, which result by far less active than their parent compounds against cancer cells. Concerning the acetylated derivatives of **7** and **10**, our data revel that their affinity for the biological target is not negatively affected by the acetylation in the positions 6, 9 and 10. The STD NMR analysis detects the interaction with the macromolecule and the theoretical results show that the carbonyl of the inserted acetyls interact through hydrogen bonds with the nucleotides, unlike the methoxy groups of **9** and **11**. The biological data show a comparable antiproliferative activity of **12** with its progenitor **10**, whereas compound **9** shows a slightly better IC_{50} than **7**. This is probably due to a better cell membrane penetration and to the intracellular hydrolysis of the acetylated appendages by esterases, which release that active form of the compounds. The DF-STD analysis of **16** show an intercalative binding mode to the DNA and hydrogen bonds with the external backbone by its hydroxy funcionalities, even though the antiproliferative activity is lower than the other compounds.

The presented results can inspire the synthesis of new DNA ligands designed for establishing additional minor groove contacts, improving the affinity for the biological target and contributing to sequence selectivity of the DNA-interacting compounds.

Acknowledgements

This research was supported by a grant of the Università degli Studi di Catania (Progetti di Ricerca di Ateneo, Catania, Italy), by MIUR, Ministero dell'Università e della Ricerca (PRIN 2006 and 2007, Rome, Italy), and by the French Cancer League, Regional Council of Burgundy.

Notes and references

1 R. D. Haworth, *J. Chem. Soc.*, 1942, 448–456.
2 J.-Y. Pan, S.-L. Chen, M.-H. Yang, J. Wu, J. Sinkkonen and K. Zou, *Nat. Prod. Rep.*, 2009, **26**, 1251–1292.
3 K.-H. Lee and Z. Xhiao, *Phytochemistry Reviews*, 2003, **2**, 341–362.
4 J. L. Charlton, *J. Nat. Prod.*, 1998, **61**, 1447–1451.
5 D. C. Ayers, and J. D. Loike, in *Lignans. Chemical, biological and clinical properties*, Cambridge University Press, Cambridge, 1990, pp 402.
6 P. M. Dewick, in *Medicinal Natural Products. A Biosynthetic Approach*, John Wiley & Sons, Chichester, UK, 2nd edn, 2001, pp. 133.
7 S. Apers, A. Vlietinck and L. Pieters, *Phytochemistry Reviews*, 2003, **2**, 201–217.
8 S. Van Miert, S. Van Dyck, T. J. Schmidt, R. Brun, A. Vlietinck, G. Lemiere and L. Pieters, *Bioorg. Med. Chem.*, 2005, **13**, 661–669.
9 A. K. Prasad, V. Kumar, P. Arya, S. Kumar, R. Dabur, N. Singh, A. K. Chhillar, G. L. Sharma, B. Ghosh, J. Wengel, C. E. Olsen and V. S. Parmar, *Pure Appl. Chem.*, 2005, **77**, 25–40.
10 S. Apers, D. Paper, J. Buergermeister, S. Baronikova, S. Van Dyck, G. Lemiere, A. Vlietinck and L. Pieters, *J. Nat. Prod.*, 2002, **65**, 718–720.
11 E. L. Ghisalberti, *Phytomedicine*, 1997, **4**, 151–166.
12 J. L. Hartwell and W. E. Detty, *J. Am. Chem. Soc.*, 1950, **72**, 246–253.
13 M. Gordaliza, M. A. Castro, J. M. Miguel del Corral and A. San Feliciano, *Curr. Pharm. Des.*, 2000, **6**, 1811–1839.
14 C. Spatafora and C. Tringali, *Targets in Heterocyclic Systems. Chemistry and Properties*, 2007, **11**, 284–312.
15 L. B. Davin, H.-B. Wang, A. L. Crowell, D. L. Bedgar, D. M. Martin, S. Sarkanen and N. G. Lewis, *Science*, 1997, **275**, 362–366.
16 C. Daquino, A. Rescifina, C. Spatafora and C. Tringali, *Eur. J. Org. Chem.*, 2009, 6289–6300.
17 (*a*) F. M. Da Cunha, D. Duma, J. Assreuy, F. C. Buzzi, R. Niero, M. M. Campos and J. B. Calixto, *Free Radical Res.*, 2004, **38**, 1241–1253; (*b*) Y.-T. Lee, M.-J. Don, P.-S. Hung, Y.-C. Shen, Y.-S. Lo, K.-W. Chang, C.-F. Chen and L.-K. Ho, *Cancer Lett.*, 2005, **223**, 19–25; (*c*) X. Debing, W. Dong, H. Yujun, X. Jiayin, Z. Zhaoyang, L. Zengpeng and X. Jiang, *Anti-Cancer Drugs*, 2006, **17**, 753–762; (*d*) H. H. Jin, P. H. Joo, C. Hwa-Jin, M. Hye-Young, P. Eun-Jung, H. Ji-Young and L. S. Kook, *J. Nutr. Biochem.*, 2006, **17**, 356–362.
18 T. Tanaka, A. Nishimura, Y. Kouno, G. Nonaka and C-R. Yang, *Chem. Pharm. Bull.*, 1997, **45**, 1596–1600.
19 S. A. Souza da Silva, A. L. Souto, M. de Fatima Agra, E. V. Leitao da-Cunha, J. M. Barbosa-Filho, M. Sobral da Silva and R. Braz-Filho, *Arkivoc*, 2004, **6**, 54–58.
20 S. Shi, Y. Zhang, K. Huang, S. Liu and Y. Zhao, *Food Chem.*, 2008, **108**, 402–406.
21 (*a*) S. Maeda, H. Masuda and T. Tokoroyama, *Chem. Pharm. Bull.*, 1994, **42**, 2506–2513; (*b*) S. Maeda, H. Masuda and T. Tokoroyama, *Chem. Pharm. Bull.*, 1995, **43**, 935–940.
22 X. Li, S. Shi, Y. Xu, Q. Tao, J. Stockhit, and Y. Zhao, CN Pat., 101024640, 2007.
23 S. Di Micco, C. Bassarello, G. Bifulco, R. Riccio and L. Gomez-Paloma, *Angew. Chem., Int. Ed.*, 2006, **45**, 224–228.
24 M. Mayer and B. Meyer, *Angew. Chem., Int. Ed.*, 1999, **38**, 1784–1788; M. Mayer and B. Meyer, *J. Am. Chem. Soc.*, 2001, **123**, 6108–6117.
25 I. Gomez-Monterrey, P. Campiglia, A. Carotenuto, D. Califano, C. Pisano, L. Vesci, T. Lama, A. Bertamino, M. Sala, A. Mazzella di Bosco, P. Grieco and E. Novellino, *J. Med. Chem.*, 2007, **50**, 1787–1798.

26 L. Martino, A. Virno, B. Pagano, A. Virgilio, S. Di Micco, A. Galeone, C. Giancola, G. Bifulco, L. Mayol and A. Randazzo, *J. Am. Chem. Soc.*, 2007, **129**, 16048–16056.
27 G. M. Morris, D. S. Goodsell, R. S. Halliday, R. Huey, W. E. Hart, R. K. Belew and A. J. Olson, *J. Comput. Chem.*, 1998, **19**, 1639–1662.
28 (*a*) H. P. Spielmann, D. E. Wemmer and J. P. Jacobsen, *Biochemistry*, 1995, **34**, 8542–8553; (*b*) J. Gallego and B. R. Reid, *Biochemistry*, 1999, **38**, 15104–15115; (*c*) A. K. Todd, A. Adams, J. H. Thorpe, W. A. Denny, L. P. G. Wakelin and C. J. Cardin, *J. Med. Chem.*, 1999, **42**, 536–540; (*d*) A. Canals, M. Purciolas, J. Aymami and M. Coll, *Acta Crystallogr., Sect. D: Biol. Crystallogr.*, 2005, **61**, 1009–1012; (*e*) A. Adams, J. M. Guss, W. A. Denny and L. P. Wakelin, *Nucleic Acids Res.*, 2002, **30**, 719–725; (*f*) J. N. Lisgarten, M. Coll, J. Portugal, C. W. Wright and J. Aymami, *Nat. Struct. Biol.*, 2001, **9**, 57–60; (*g*) X. Shui, M. E. Peek, L. A. Lipscomb, A. P. Wilkinson, L. D. Williams, M. Gao, C. Ogata, B. P. Roques, C. Garbay-Jaureguiberry, A. P. Wilkinson and L. D. Williams, *Curr. Med. Chem.*, 2000, **7**, 59–71; (*h*) H. Robinson, W. Priebe, J. B. Chaires and A. H. Wang, *Biochemistry*, 1997, **36**, 8663–8670.
29 *MacroModel*, version 8.5, Schrödinger LLC, New York, NY, 2003.
30 W. D. Cornell, P. Cieplak, C. I. Bayly, I. R. Gould, K. M. Merz Jr, D. M. Ferguson, D. C. Spellmeyer, T. Fox, J. W. Caldwell and P. A. Kollman, *J. Am. Chem. Soc.*, 1995, **117**, 5179–5197; P. K. Weiner and P. A. Kollman, *J. Comput. Chem.*, 1981, **2**, 287–303; S. J. Weiner, P. A. Kollman, D. A. Case, U. C. Singh, C. Ghio, G. Alagona, S. Profeta Jr and P. K. Weiner, *J. Am. Chem. Soc.*, 1984, **106**, 765–784; S. J. Weiner, P. A. Kollman, D. T. Nguyen and D. A. Case, *J. Comput. Chem.*, 1986, **7**, 230–252.
31 W. C. Still, A. Tempczyk, R. C. Hawley and T. Hendrickson, *J. Am. Chem. Soc.*, 1990, **112**, 6127–6129.
32 T. A. J. Halgren, *J. Comput. Chem.*, 1996, **17**, 616–641.
33 P. J. Goodford, *J. Med. Chem.*, 1985, **28**, 849–857.
34 M. F. Sanner, *J. Mol. Graphics Mod.*, 1999, **17**, 57–61.
35 M. F. Sanner, A. J. Olson and J. C. Spehner, *Biopolymers*, 1996, **38**, 305–320.

